IET Electric Power Applications

The Institution of Engineering and Technology WILEY

DC-link low-frequency current and voltage ripple analysis in multiphase voltage source inverters with unbalanced load

Marija Vujacic[1] | **Obrad Dordevic[2]** | **Riccardo Mandrioli[1]** | **Gabriele Grandi[1]**

[1]Department of Electrical, Electronic and Information Engineering, University of Bologna, Bologna, Italy

[2]School of Engineering, Liverpool John Moores University, Liverpool, UK

Correspondence

Obrad Dordevic, School of Engineering, Liverpool John Moores University, Byrom St, Liverpool L3 3AF, UK.
Email: O.Dordevic@ljmu.ac.uk

Present address

Marija Vujacic, Grid Automation, Hitachi Energy, Via Albareto 35, 16153 Genova, Italy.

Abstract

Inverter's performance and operating mode may be negatively affected by inverter input (dc-link) current and voltage ripple. It is a common experience that even theoretically balanced loads with perfectly balanced supply voltages, such as multiphase ac motors supplied by pulse-width modulation (PWM) inverters, in practice show a certain degree of current unbalance, in the range of a few percent, which introduces a low-frequency instantaneous power oscillation. This reflects in current and voltage low-frequency ripple on the dc-link inverter side (i.e. at the double-fundamental frequency). A possible method to analyse this matter is through the symmetric sequence components. In particular, based on the first negative current sequence component and by considering the equivalent dc-link impedance calculated at the dominant double-fundamental frequency, the amplitude of the corresponding dc-link voltage ripple component is calculated in this work for a general multiphase load. Finally, the design of the dc-link capacitor in multiphase inverters is proposed considering requirements referred to the double-fundamental dc voltage ripple. The feasibility of the proposed developments has been verified for three-, five- and seven-phase inverters by both numerical simulations and comprehensive experimental tests, always showing a good matching.

KEYWORDS

DC-AC power converters, DC-bus voltage ripple, DC-link capacitor, electric motor drive, multiphase systems, pulse-width modulation, switching circuits, voltage-source inverter

1 | INTRODUCTION

During the last decades, multiphase variable speed drives have gained widespread attention, and numerous interesting developments have been published recognising their advantages over the standard three-phase solutions [1–3]. Multiphase machines are usually fed by two-level multiphase voltage source inverters (VSIs). Hence, great attention has been focussed on the development of new topologies and control strategies of multiphase inverters. Research activities are mostly related to the analysis of output inverter quantities (currents and voltages), but attention has been paid to the input (dc-link) side of the inverters as well. Regarding the output side of the inverters, the output current ripple is studied in terms of root mean square (RMS) minimisation and its maximum peak-to-peak value [4–7].

The analysis of the inverter's input variables is particularly important for the dc-link capacitor sizing since the required capacitance is usually determined by the values of the dc-link current and voltage ripple. The dc-link voltage ripple can lead to an increase in electric losses, an excessive rise of the motor temperature, the appearance of the torque pulsation etc. [8]. In general, a large dc-link capacitor can significantly reduce the voltage ripple, and smooth dc-link voltage can be obtained. As a consequence, the dc-link capacitors are often oversized. Such heavy and bulky capacitors can become a critical obstacle to the high power density of the inverter system. Therefore, there is a general requirement to keep the size of the dc-link capacitor as small as possible.

Most of the analyses of the input (dc-link) side of inverters refer to two-level three-phase topology with balanced loads.

The input current analyses are usually based on the spectral (harmonic) analysis [9, 10] and RMS calculations [11, 12]. The design of the dc-link capacitor based on the maximum (peak-to-peak) value of the dc voltage switching ripple and assuming ideal symmetrical load is shown in Ref. [13].

The effect of unbalanced load conditions on the dc-link current and voltage ripples has been investigated in Ref. [14] for three-phase inverters. In general, any deviation of voltage and current waveforms from symmetric sinusoidal disposition, in terms of magnitude, phase angle, or both magnitude and phase angle, is considered as unbalance. The current unbalance and its associated power unbalance appear as a result of un-balanced magnitudes of the phase voltages, angle displacement between the phase voltages or internal impedances of the motor. The impedance unbalances in the motor may have been caused by unbalanced heating of the stator [15]. Motor un-balance can also be due to a manufacturing problem such as the unequal number of turns in the windings, a misaligned rotor or an asymmetric stator. Sometimes, to reduce the time and lower the repair process costs, failed windings are repaired by isolating the failed turn, thus reducing the impedance of the repaired phase. Extreme examples of the current unbalance are non-disruptive faults. Faults usually cause temporary current unbalance and, if they are not repaired on time, these conditions may cause system instability [16].

For grid-connected applications, the impact of the ac voltage unbalance on the lifetime of dc-link capacitors has been shown in Ref. [17]. The analysis of dc-bus capacitor current ripple and the resulting thermal stress have been presented for an adjustable speed drive system under input voltage unbalance and sag conditions in Ref. [18]. It is shown that a voltage unbalance in the range of 2.5% results in halving of the dc-link capacitor's lifetime if the unbalanced condition persists.

Regarding the two-level multiphase VSIs, a generalised approach towards the dc-link voltage switching ripple analysis has been presented in Ref. [19]. The guideline for designing a dc-link capacitor, based on the maximum (peak-to-peak) value of the dc-link voltage ripple, has been provided considering balanced loads. The impact of different pulse-width modulation (PWM) modulation strategies on the RMS value of the dc current has been studied for a dual-three phase induction machine in Refs. [20, 21]. Referring to the five-phase case, input current and voltage ripple RMS calculations are reported in Ref. [22]. The dc-link voltage ripple amplitude is calculated in Refs. [23, 24], and the dc-link capacitor design is proposed based on the dc-link voltage switching ripple requirements for five- and seven-phase inverters, respectively. The impact of the number of phases on input current ripple has been analysed in Ref. [25]. So far, all analyses of the dc-link variables in multi-phase inverters have been based on the assumption of the balanced load conditions. No studies have dealt with the impact of load unbalances on the input current and voltage ripple in two-level n-phase inverters ($n > 3$).

In this work, the dc-link current and voltage ripple analysis for two-level multiphase VSIs have been presented considering slightly unbalanced load conditions, assuming balanced inverter output voltages. Namely, the load can be a standard multiphase ac motor, showing in practice a certain degree of unbalance, in order of a few percent. An example of such a small unbalance in an ac motor is the line-to-line motor resistance which differs up to 2% compared to the average. Consequently, depending on the load power and percentage of the unbalance, an instantaneous power oscillation (at the double-fundamental frequency) is introduced, reflecting in current and voltage low-frequency ripples on the dc-link capacitor. In the following, the amplitudes of the two low-frequency dc-link ripple components have been analytically investigated. First, two most commonly used transformations for analysing multiphase systems – Fortescue's (symmetrical components) and multiple space vectors – have been briefly reviewed in Section 2. The amplitude of the double-fundamental voltage ripple component has been calculated in Section 3 and, based on it, a simple guideline for designing the dc-link capacitor is proposed in Section 4. Numerical simula-tions are carried out utilising Matlab/Simulink, and experi-mental tests are performed for three-, five- and seven-phase inverters aiming to verify analytical developments. The results are shown in Section 5. Finally, a brief discussion of the pre-sented results is given in the conclusion.

2 | BASIC DEFINITIONS AND TRANSFORMATIONS FOR MULTIPHASE SYSTEMS

The multiphase VSI topology supplying a star-connected passive- and/or motor-load is presented in Figure 1.

Assuming that x_k are real quantities related to the n-phase system ($k = 1, 2, …, n$) with sinusoidal waveforms and the same frequency, the n phasors $\mathbf{X}_k = \mathrm{X}_k e^{-j\varphi_k}$ are introduced as

$$[\mathbf{X}] = (\mathbf{X}_1, \mathbf{X}_2, …, \mathbf{X}_n), \tag{1}$$

according to

$$x_k(t) = \sqrt{2}\, \mathrm{X}_k \cos(\omega t - \varphi_k) = \mathrm{Re}\left[\sqrt{2}\, \mathbf{X}_k e^{j\omega t}\right], \tag{2}$$

where $\mathbf{X}_k$ is the RMS value of $x_k(t)$ over the fundamental period $T = 2\pi/\omega$, and φ_k is the phase angle. Note that phasors and vectors are denoted here with bold non-italic fonts.
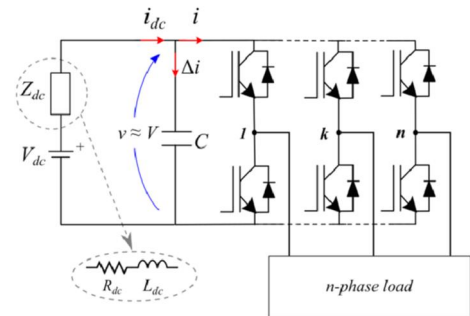

FIGURE 1 Circuit scheme of n-phase voltage source inverter

If the direct Fortescue's transformation is applied to Equation (1), the n symmetrical sequence components are obtained:

$$[\mathbf{X}_S] = [\mathbf{X}_0, \mathbf{X}_{+1}, \ldots, \mathbf{X}_{+r}, \mathbf{X}_{-r}, \ldots, \mathbf{X}_{-1}], \qquad (3)$$

being $r = (n–1)/2$ (for odd n), and the direct transformation defined as [26]:

$$\mathbf{X}_{\pm h} = \frac{1}{n} \sum_{k=1}^{n} \mathbf{X}_k \alpha^{\pm h(k-1)}, \ h = 0, \ 1, \ 2, \ldots, r, \qquad (4)$$

where $\alpha = e^{j(2\pi/n)}$.

The inverse transformation is given by

$$\mathbf{X}_k = \sum_{h=-r}^{r} \mathbf{X}_h \alpha^{-h(k-1)}, \ k = 1, \ 2, \ldots, n. \qquad (5)$$

The previous transformations can be rewritten in a compact matrix form as follows

$$[\mathbf{X}_S] = [\alpha]^{-1}[\mathbf{X}], \qquad (6)$$

$$[\mathbf{X}] = [\alpha][\mathbf{X}_S], \qquad (7)$$

where,

$$[\alpha]^{-1} = \frac{1}{n} \begin{bmatrix} 1 & 1 & 1 & \cdots & 1 \\ 1 & \alpha & \alpha^2 & \cdots & \alpha^{n-1} \\ 1 & \alpha^2 & \alpha^4 & \cdots & \alpha^{n-2} \\ \vdots & \vdots & \vdots & \ddots & \vdots \\ 1 & \alpha^{n-1} & \alpha^{n-2} & \cdots & \alpha \end{bmatrix}, \qquad (8)$$

$$[\alpha] = \begin{bmatrix} 1 & 1 & 1 & \cdots & 1 \\ 1 & \alpha^{-1} & \alpha^{-2} & \cdots & \alpha \\ 1 & \alpha^{-2} & \alpha^{-4} & \cdots & \alpha^2 \\ \vdots & \vdots & \vdots & \ddots & \vdots \\ 1 & \alpha & \alpha^2 & \cdots & \alpha^{n-1} \end{bmatrix}. \qquad (9)$$

Another transformation most commonly used for analysing multiphase systems, due to the broader generality compared to Fortescue's, is 'space vector' transformation. For the n-phase system, multiple space vector transformation and inverse transformation can be defined as [26]:

$$x_0 = \frac{1}{n} \sum_{k=1}^{n} x_k, \qquad (10)$$

$$\mathbf{x}_h = \frac{2}{n} \sum_{k=1}^{n} \mathbf{x}_h \alpha^{h(k-1)}, \ h = 1, \ 2, \ldots, r, \qquad (11)$$

$$x_k = x_0 + \sum_{h=1}^{r} \mathbf{x}_h \alpha^{h(k-1)}, \ k = 1, \ 2, \ldots, n. \qquad (12)$$

In order to show the relation between two previously reviewed transformations, symmetrical sequence, and space vector transformations, for n sinusoidal waveforms with the same frequency, the quantities given by Equation (2) are rewritten in the following form [26]:

$$x_k = \frac{\sqrt{2}}{2} \left(\mathbf{X}_k e^{j\omega t} + \mathbf{X}_k^* e^{-j\omega t} \right), \quad k = 1, \ 2, \ 3, .., n. \qquad (13)$$

Applying Equations (10) and (11) to Equation (13), and considering Equation (4), yields

$$x_0 = \mathrm{Re}\left[\sqrt{2} \ \mathbf{X}_0 e^{j\omega t} \right], \qquad (14)$$

$$\mathbf{x}_h = \sqrt{2} \mathbf{X}_{+h} \ e^{j\omega t} + \sqrt{2} \mathbf{X}_{-h}^* e^{-j\omega t}, \quad h = 1, \ 2, \ldots, r, \qquad (15)$$

which represents the relationship between two considered transformations.

3 | DC-LINK LOW-FREQUENCY CURRENT AND VOLTAGE RIPPLE ANALYSIS IN CASE OF LOAD UNBALANCE

Regarding n-phase inverter/load and multiple space vector definition given by Equation (11), the instantaneous power can be expressed in terms of space vector components as [26]:

$$p = n \, v_0 i_0 + \frac{n}{2} \sum_{h=1}^{r} \mathbf{v}_h \cdot \mathbf{i}_h, \quad h = 1, \ 2, \ldots, r. \qquad (16)$$

It can be noted that only the current and load voltage components of the same sequence interact. Hence, the instantaneous power can be written as the sum of contributions of each sequence as follows:

$$p = \sum_{h=0}^{r} p_h, \qquad (17)$$

being

$$p_0 = n \, v_0 i_0, \qquad (18)$$

$$p_h = \frac{n}{2} \mathbf{v}_h \cdot \mathbf{i}_h = \frac{n}{2} \mathrm{Re}\left[\mathbf{v}_h \mathbf{i}_h^* \right], \quad h = 1, \ 2, \ldots, r. \qquad (19)$$

The direct rotating component of the voltage space vector is equal in magnitude to $\sqrt{2}$ times the magnitude of the positive symmetrical component of the first sequence. Referring to Equation (15), it can be expressed as follows:

$$\mathbf{v}_1 = \sqrt{2} \, \mathbf{V}_{+1} e^{j\omega t} = \sqrt{2} \, V_{+1} e^{j\omega t}. \qquad (20)$$

Due to unbalanced load conditions and applying Equation (15) to the phase current, yields

$$\mathbf{i}_b = \sqrt{2}\,\mathbf{I}_{+b}e^{j\omega t} + \sqrt{2}\,\mathbf{I}_{-b}^*e^{-j\omega t}, \qquad (21)$$

being $\mathbf{I}_{+b} = I_{+b}e^{-j\varphi_{+1}}$ and $\mathbf{I}_{-b} = I_{-b}e^{-j\varphi_{-1}}$.

Since multiphase loads/motors without the neutral wire are considered in this work, no homopolar (common mode) current component i_0 can circulate, that is, the zero sequence component of the current is $\mathbf{I}_0 = 0$.

Because of the interaction between current and voltage components of the same sequence, and due to the existence of only first positive and zero sequence load voltage components, only current components $\mathbf{I}_{+1}$ and $\mathbf{I}_{-1}$ contribute to the instantaneous power. Introducing Equations (20) and (21) in Equation (19), the instantaneous power becomes

$$p = n\left[V_{+1}I_{+1}\cos\varphi_{+1} + V_{+1}I_{-1}\cos(2\omega t - \varphi_{-1})\right]. \quad (22)$$

Note that although the zero sequence load voltage component is non-zero in case of unbalanced loads, it does not contribute to the instantaneous power.

Considering the input/output power balance and assuming an ideal (lossless) inverter, one can write

$$V\bar{i} = p, \qquad (23)$$

where $\bar{i}$ is the input dc-link current averaged over the switching period T_{sw}, and V is the dc-link voltage. Note that the averaged input current corresponds to the inverter input current without the switching component.

The first positive voltage sequence component can be introduced as a function of the modulation index m as follows:

$$V_{+1} = \frac{mV}{\sqrt{2}}. \qquad (24)$$

Considering Equations (22) and (24), the averaged input current component can be obtained by Equation (23) as follows:

$$\bar{i} = I_{dc} + \tilde{i} = \frac{nm}{\sqrt{2}}\left[I_{+1}\cos\varphi_{+1} + I_{-1}\cos(2\omega t - \varphi_{-1})\right]. \quad (25)$$

The dc (I_{dc}) and low-frequency ($\tilde{i}$) current components can be readily obtained from Equation (25) as follows:

$$I_{dc} = \frac{n}{\sqrt{2}}mI_{+1}\cos\varphi_{+1}, \qquad (26)$$

$$\tilde{i} = \frac{n}{\sqrt{2}}mI_{-1}\cos(2\omega t - \varphi_{-1}). \qquad (27)$$

Based on Equation (27) and introducing unbalance factor (U_F) defined as the ratio of the magnitude of the negative current sequence component to the magnitude of the positive current sequence component and given by [27]:

$$U_F = \frac{I_{-1}}{I_{+1}}, \qquad (28)$$

The amplitude of the low-frequency dc-link current component, which appears at double the fundamental frequency, can be expressed as follows:

$$\tilde{I}_{pk} = n\,I_{+1}\,m\frac{U_F}{\sqrt{2}}. \qquad (29)$$

It can be noted in Equation (29) that the amplitude increases by increasing the number of phases (n) if the same output current is assumed. However, for a fair comparison of inverter topologies with different phase numbers, the same apparent output power should be considered instead. Under such an assumption, the double-fundamental dc current ripple amplitude is affected only by the unbalance factor.

The low-frequency voltage ripple component ($\tilde{v}$) can be calculated based on Equation (27), introducing the dc-link equivalent impedance with magnitude $Z_{2\omega}$ and phase angle φ_z:

$$\tilde{v} = Z_{2\omega}\frac{n}{\sqrt{2}}m\,I_{-1}\cos(2\omega t - \varphi_{-1} + \varphi_z). \qquad (30)$$

Subscript 2ω stands to highlight that the frequency at which the impedance is calculated is twice the angular fundamental frequency $\omega = 2\pi f$. The equivalent impedance is calculated as the parallel between the dc source impedance Z_{dc} and the reactance of the dc-link capacitor C_{dc}. The following equations are obtained for the magnitude and the phase angle of the dc-link equivalent impedance:

$$Z_{2\omega} = \frac{1}{2\omega C_{dc}}\sqrt{\frac{R_{dc}^2 + (2\omega L_{dc})^2}{R_{dc}^2 + \left(2\omega L_{dc} - \frac{1}{2\omega C_{dc}}\right)^2}}, \qquad (31)$$

$$\varphi_z = \text{arctg}\left[\frac{2\omega L_{dc}}{R_{dc}}\left(1 - 4\omega^2 L_{dc}C_{dc} - \frac{R_{dc}^2 C_{dc}}{L_{dc}}\right)\right], \qquad (32)$$

where R_{dc} and L_{dc} are the dc source series resistance and series inductance, respectively (refer to Figure 1).

Finally, the amplitude or the peak value of the low-frequency voltage ripple component is given by

$$\tilde{V}_{pk} = Z_{2\omega}\tilde{I}_{pk}. \qquad (33)$$

The amplitude or the peak value of $\tilde{V}$ can also be expressed as a function of unbalance factor considering Equation (29) as

$$\tilde{V}_{pk} = n\,I_{+1}\,m\frac{U_F}{\sqrt{2}}\,Z_{2\omega}. \qquad (34)$$

The expression in Equation (34) is compact. However, the assessment of current sequence components becomes more complex by increasing the number of phases, as shown in the following.

4 | DC-LINK CAPACITOR DESIGN

The design of the dc-link capacitor in multiphase inverters is proposed considering requirements referred to the amplitude of dc voltage ripple component calculated in the previous section (at the double-fundamental frequency).

According to Equation (34), the dc-link low-frequency voltage ripple component depends on the total dc-link impedance calculated at the double-fundamental frequency and on the unbalance factor. Taking into consideration Equation (31), the amplitude of the corresponding dc-link voltage ripple is finally expressed as follows:

$$\tilde{V}_{pk} = \frac{n}{\sqrt{2}} m I_{+1} U_F \frac{1}{2\omega C_{dc}} \sqrt{\frac{R_{dc}^2 + (2\omega L_{dc})^2}{R_{dc}^2 + \left(2\omega L_{dc} - \frac{1}{2\omega C_{dc}}\right)^2}}. \tag{35}$$

The expression given by Equation (35) can be used for dc-link capacitor sizing. However, Equation (35) shows rather bulky calculations. A reasonable simplification can be introduced in case of a high dc source impedance. In such a case, the dc-link equivalent impedance can be approximated as follows:

$$Z_{2\omega} \approx \frac{1}{2\omega C_{dc}}. \tag{36}$$

Hence, under the above assumption, the amplitude of the double-fundamental dc voltage ripple Equation (35) can be simplified as follows:

$$\tilde{V}_{pk} = \frac{n}{\sqrt{2}} m I_{+1} U_F \frac{1}{2\omega C_{dc}}. \tag{37}$$

Finally, given $\tilde{V}_{pk}$ and the unbalance factor U_F as a condition, the dc-link capacitor can be designed using the following expression:

$$C_{dc} \geq \frac{n}{\sqrt{2}} m I_{+1} U_F \frac{1}{2\omega \tilde{V}_{pk}}. \tag{38}$$

It can be concluded that from the point of view of the dc-link capacitor sizing, if the same apparent power is considered within compared multiphase inverter topologies, there are no benefits of increasing the number of phases because the amplitude of the low-frequency voltage ripple component depends only on the level of unbalance (U_F). On the other side, considering the dc-link voltage switching

ripple (high-frequency), it has been shown in Ref. [19] that its maximum value decreases when the number of phases increases up to $n = 7$ and then practically saturates for $n > 7$. In applications where both the switching frequency and the unbalance factor are small, both the switching and the low-frequency dc-link voltage ripple components should be calculated. Based on a dominant component and the specific requirements (limits), either the expression in Equation (16) from Ref. [19] or Equation (38) should be applied for the dc-link capacitor design. In general, the higher calculated capacitor value should be chosen. Further guidelines on designing the dc-link capacitor in the case of balanced loads can be found in Refs. [13, 23, 24] for different converter topologies.

It is worth mentioning that in this work, it is assumed that the only low-frequency current harmonics source is actually the inverter. At this stage, harmonic content attributable to a supply rectifier or other converters sharing the same dc-link is assumed to be negligible or filtered out by the dc source impedance. If the latter assumption is not valid, the current harmonics should be combined, and the results presented in this work should be considered as a starting point for determining the total low-frequency dc-link voltage harmonics.

5 | RESULTS

Numerical simulations and experimental tests are carried out to verify the analytical developments for multiphase inverters with an odd number of phases. Tests have been performed for two-level three-, five- and seven-phase inverters. Utilised three-phase loads in the experiments were two standard induction motors (IMs) at standstill, with their intrinsic small unbalance. Slightly unbalanced R–L loads were used for obtaining the experimental results for the five- and seven-phase cases. Reference is made to sinusoidal PWM to generate the firing signals. Simulation results have been obtained using Matlab/ Simulink, and all parameters were adjusted to the corresponding values of the experimental setup. In order to point out the effects of the dead-time on the dc-link quantities, additional simulations have been carried out when the dead-time is considered (as in the experiments) and when it is set to zero (ideal commutation).

5.1 | Three-phase inverter

First, the experimental tests were performed using a three-phase custom-made inverter with the Mitsubishi PS22A76 intelligent power IGBT module. The DSP microcontroller board controlled the inverter through an optical interface board. DSP board TMS320F28379D is programmed by Code Composer Studio (CCS), with the possibility of real-time adjustment of modulation parameters by the computer interface. The dc source impedance was added between the external dc source and the dc-link having the following parameters:

$R_{dc} = 5.5\ \Omega$ and $L_{dc} = 27$ mH. The dc-link film capacitor has the value $C_{dc} = 100\ \mu$F. The inverter hardware-implemented dead-time value is 4 μs while the switching frequency is set to 2.5 kHz to make the dead-time effect almost negligible (i.e. 1% of the switching period). A general view of the experimental setup is shown in Figure 2.

Measurements have been taken using two standard (commercial) star-connected three-phase induction motors (at standstill) shown in Figure 3. The parameters of the motors are measured by the LCR meter Agilent 4263B, and they are shown in Table 1. The RMS values of the phase currents are measured by digital clamp meter and summarised in Table 2. The resulting current sequence components and the intrinsic unbalances are given in Table 3.

The current sequence components are calculated from the RMS values of the phase currents as [28]:

$$I_{-1} = \sqrt{\frac{2}{3}\left[\left(I_1 - I_{avg}\right)^2 + \left(I_2 - I_{avg}\right)^2 + \left(I_3 - I_{avg}\right)^2\right]}, \quad (39)$$

being
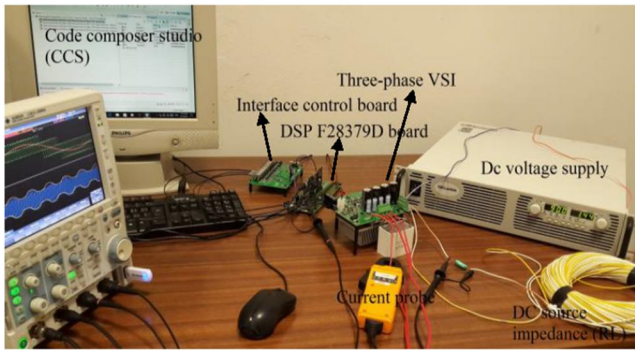
FIGURE 2 Experimental setup for the three-phase system
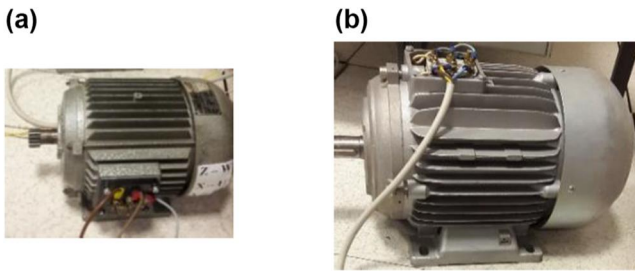
(a)   **(b)**

FIGURE 3 The two standard (commercial) three-phase inductor motors (IMs): (a) 0.5-kW three-phase IM-1 and (b) 4-kW three-phase IM-2

TABLE 1 Motor load parameters (standstill)

	0.5-kW three-phase IM-1	4-kW three-phase IM-2
R (Ω)	26.8	3.16
L (mH)	103	20
φ	50°	60°

Abbreviation: IM, inductor motor.

$$I_{+1} \approx I_{avg} = \frac{1}{3}\left(I_1 + I_2 + I_3\right). \quad (40)$$

Obtained values are set in simulations to provide a fair comparison between analytical calculations, simulations, and experimental results.

The first set of measurements was done considering a 0.5 kW three-phase inductor motor (IM-1). The simulation and experimental results are shown in Figures 4 and 5, respectively. Note that an accurate measurement procedure is essential to avoid any false problems in further analysis.

Figure 4 shows the instantaneous dc-link voltage with subtracted dc component (blue trace) together with its averaged value over the switching period (red trace). The averaged value is obtained by applying a moving average that filters out the high-frequency ripple. Note that without the unbalance, the

TABLE 2 Measured current values and dc supply voltages for the two induction motors (standstill)

	0.5-kW three-phase IM-1	4-kW three-phase IM-2
V_{dc} (V)	98.8	50.2
m	0.50	0.50
I_1 (A)	0.749	2.241
I_2 (A)	0.763	2.256
I_3 (A)	0.768	2.230

Abbreviation: IM, inductor motor.

TABLE 3 Current sequence components, unbalance factor and comparison within the dc voltage ripple amplitudes for the two induction motors (standstill)

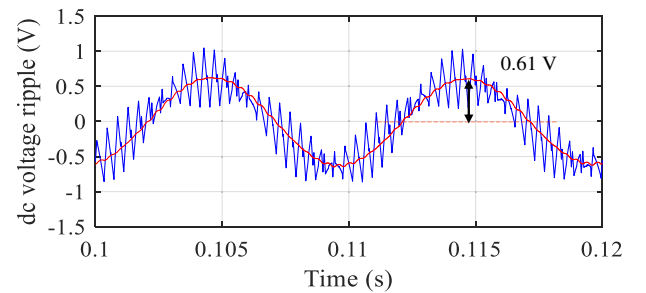|	0.5-kW three-phase IM-1	4-kW three-phase IM-2
I_{+1} (A)	0.760	2.242
I_{-1} (A)	0.01137	0.01507
U_F (%)	1.5	0.68
ana. $\tilde{V}_{pk}$ (V)	0.61	0.81
sim. $\tilde{V}_{pk}$ (V)	0.61	0.81
exp. $\tilde{V}_{pk}$ (V)	0.57	0.78

Abbreviation: IM, inductor motor.

FIGURE 4 Simulation results: The total instantaneous dc-link voltage ripple (blue trace) and its averaged value over T_{sw} (red trace) in case of three-phase IM-1

dc-link voltage would have assumed the waveform analysed in Ref. [19], that is, the switching ripple only.

The experimental results are shown in Figure 5 by Yoko-gawa DLM 2024 oscilloscope screenshot. The upper (blue) trace presents the total dc-link voltage ripple. The dc (average) voltage component was taken away by using the 'ac coupling' function of the oscilloscope. The bottom (pink) trace presents the low-frequency dc-link voltage ripple component, obtained by filtering the total dc-link voltage ripple with a built-in low-pass filter of the oscilloscope. The measured alternating dc-link voltage component's amplitude is slightly lower than the simulation results due to non-ideal measuring equipment.

In order to point out the effects of the dead-time, Figure 6 reports the harmonic spectra of the dc-link voltage ripple considering the original simulation (no dead-time, pink histo-gram) and a realistic case with the same dead-time adopted as in the experiments (4 μs, blue histogram). The harmonic amplitude is also expressed in % of the dc voltage component with a second scale placed on the right-hand side of the dia-gram (the same also applies to all the following graphs with spectra).

As it can be noted, the dead-time itself does not introduce significant low-order harmonics, apart from a small sixth order component, as reported in Ref. [29]. A small reduction in the second order harmonic component can also be justified by a small reduction in the output voltage/current introduced by the dead-time, as reported in Refs. [30, 31].

The second set of measurements was done considering a 4 kW three-phase induction motor (IM-2). The same

procedure has been followed as for the first set of measure-ments. The simulation and experimental results are shown in Figures 7 and 8, respectively, and the comparison with/without dead-time in Figure 9.

Figure 7 shows the instantaneous dc-link voltage with subtracted dc component (blue trace) together with its aver-aged value over the switching period (red trace).

The experimental results are shown in Figure 8. The upper (blue) trace presents the total dc-link voltage ripple, whereas the bottom (pink) trace shows the low-frequency ripple component.

Similar to Figure 6, numerical harmonic spectra in case of no dead-time (pink) and realistic dead-time (blue) are reported in Figure 9 in case of IM-2. Comments are practically the same.

Parameters of interest are summarised in Table 3 for the two considered three-phase cases. The unbalance factor (U_F) is calculated by Equation (28), and the amplitude of the low-frequency voltage ripple component is calculated by Equation (33). It can be noted that the results show a good matching for all considered cases.

5.2 | Five- and seven-phase inverters

The experimental setup is shown in Figure 10. It consists of a two-level custom-made inverter with eight legs (up to eight output phases), and it has been used for experiments with five- and seven-phase symmetrical R–L load. The employed IGBT module is the FS50R12KE3 (Infineon). The inverter was controlled by dSpace ds1006 real-time system. The dc-bus supply voltage is provided from the external dc source Sor-ensen SGI 600/25. The Z_{dc} impedance is added between the dc source and the dc-link. The equivalent value of two dc-link
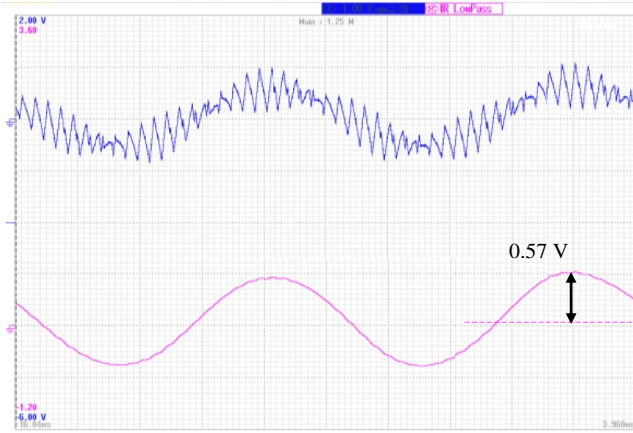

FIGURE 5 Experimental results (three-phase IM-1): Total dc-link voltage ripple (blue trace) and low-frequency (filtered) voltage ripple component (pink trace)
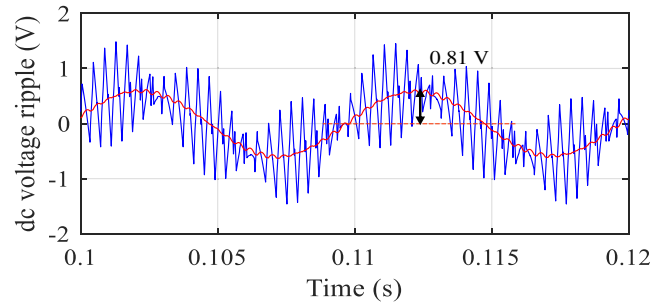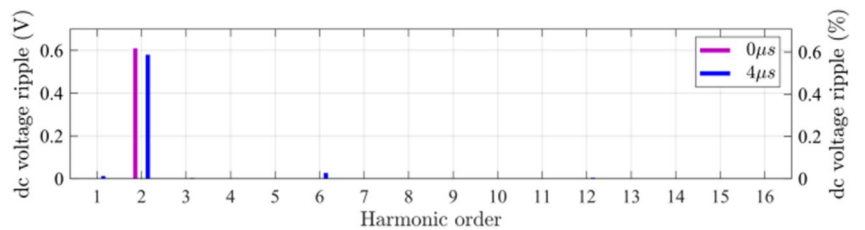

FIGURE 7 Simulation results: The total instantaneous dc-link voltage ripple (blue trace) and its averaged value over T_{sw} (red trace) in case of three-phase IM-2

FIGURE 6 Harmonic spectra of the dc-link voltage ripple in case of three-phase IM-1 considering no dead-time (pink lines) and 4 μs dead-time (blue lines)

film capacitors connected in parallel is 209 μF. The inverter dead-time is 6 μs and the switching frequency is set to 2 kHz for the same reason given above for the three-phase case. In this way, the dead-time is limited to 1.2% of the switching period.

The simulation and experimental setup parameters are summarised in Table 4. The two power phase angles of interest are obtained using two different sets of passive balanced R–L load impedances. The load parameters are given in Table 5. The unbalance was introduced by adding the resistor $R_0 = 4.5\ \Omega$ in series with one of the phases. Since the unbalance factor U_F does not depend on the current sequence phase angle (see Equation (28)), the same set of unbalances used in this subsection could have been generated by employing a virtually infinite combination of unbalancing impendences.

5.2.1 | Five-phase

In the case of a five-phase inverter supplying a five-phase R–L load, the dc-link voltage ripple across the dc-link capacitor was measured by Tektronix P5205A, 100 MHz, high voltage differential probe.

To verify the amplitude of the low-frequency voltage ripple component, the total dc-link voltage was treated by applying a
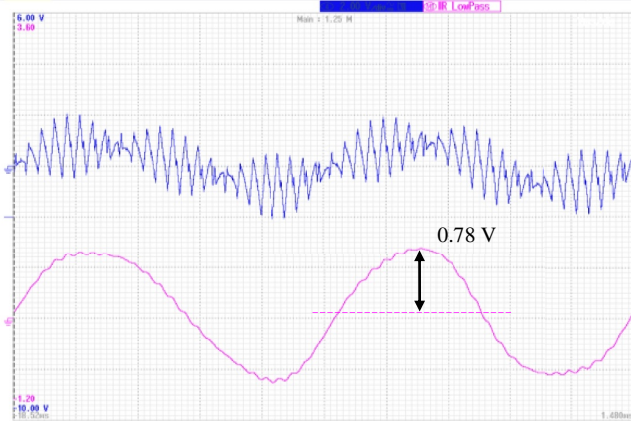
moving average filter in post-processing of the experimental data. Numerical simulations (pink traces) and experimental results (blue traces) are shown from Figures 11–14, presenting the total dc-link voltage ripple (left column) and its double-fundamental (filtered) component (right column). The harmonic spectra in the case of the original simulations (no dead-time, pink lines) and 6 μs dead-time (blue lines) are reported in the bottom histograms. Two values of modulation index ($m = 0.25$ and $m = 0.5$) and two output phase angles ($\varphi = 20°$ and $\varphi = 70°$) are considered.

The current sequence components have been calculated from the measured RMS values of the phase currents by applying Fortescue's transformation. The amplitude of the low-frequency voltage ripple component is calculated based on the first negative current sequence component and by considering the dc-link equivalent impedance $Z_{2\omega}$ given by Equation (31). Finally, the unbalance factor is calculated. Parameters of interest and analytically calculated amplitudes of the low-frequency voltage ripple component in different operating conditions are summarised in Table 6, together with

FIGURE 8 Experimental results (three-phase IM-2): total dc-link voltage ripple (blue trace) and low-frequency (filtered) voltage ripple component (pink trace)
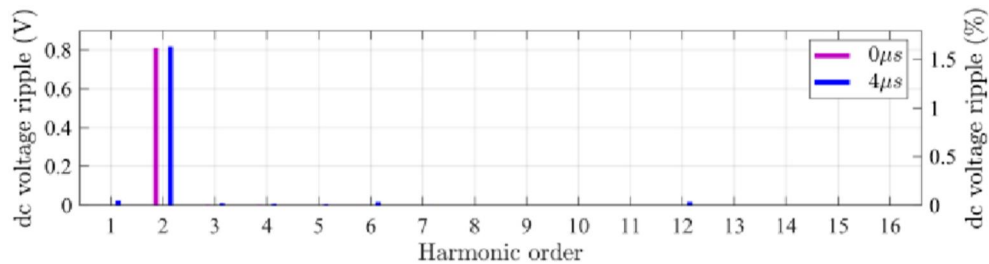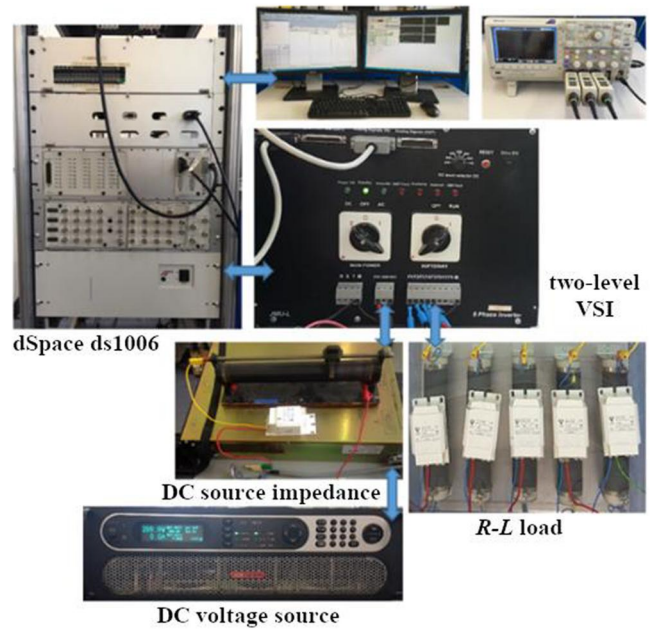

FIGURE 10 Experimental setup for the five- and seven-phase systems

FIGURE 9 Harmonic spectra of the dc-link voltage ripple in case of three-phase IM-2 considering no dead-time (pink lines) and 4 μs dead-time (blue lines)

the corresponding simulations and experimental results. Only the first current sequence components (both positive, and negative, + and −) are introduced since they were only of interest for the calculations.

Concerning the dead-time, also in the case of five-phase inverter, the effect on the low-order harmonics of the dc-link voltage is almost negligible, as in case of the three-phase inverter. In fact, apart from small numerical noises, only a

TABLE 4 Simulation and experimental setup parameters

Parameter	Symbol	Value
DC voltage supply	V_{dc}	300 V
DC source resistance	R_{dc}	5.3 Ω
DC source inductance	L_{dc}	4.5 mH
DC-link capacitance	C_{dc}	209 μF
Equivalent series resistance (C_{dc})	ESR	30 mΩ
Fundamental frequency	f	50 Hz
Switching frequency	f_{sw}	2 kHz

TABLE 5 Passive R–L load parameters with different phase angles

φ	20°	70°
R (Ω)	24	24
L (mH)	25	204

10th order component is noticeable. Also in this case, the small reduction in the second order harmonic component can be justified by the small reduction in the output voltage/current introduced by the dead-time [30, 31].

5.2.2 | Seven-phase

In the case of a seven-phase inverter supplying a seven-phase R–L load, the experimental data are post-processed in the same way as explained before for the five-phase inverter.

Numerical simulations (pink traces) and experimental results (blue traces) are shown from Figures 15–18, presenting the total dc-link voltage ripple (left column) and its filtered double-fundamental component (right column).

The harmonic spectra in case of the original simulations (no dead-time, pink lines) and 6 μs dead-time (blue lines) are reported in the bottom histograms.

For the sake of comparison, parameters of interest and the analytically calculated and measured amplitudes of the dc low-frequency voltage ripple component in different operating conditions are summarised in Table 7. Also, the first current sequence components (+ and −) and unbalance factor are calculated for all considered operating conditions. It can be noted that a satisfactory matching is achieved between the results confirming the analytical developments.

Concerning the dead-time, also in the case of seven-phase inverter, the effect on the low-order harmonics of the dc-link voltage is almost negligible, as in case of the
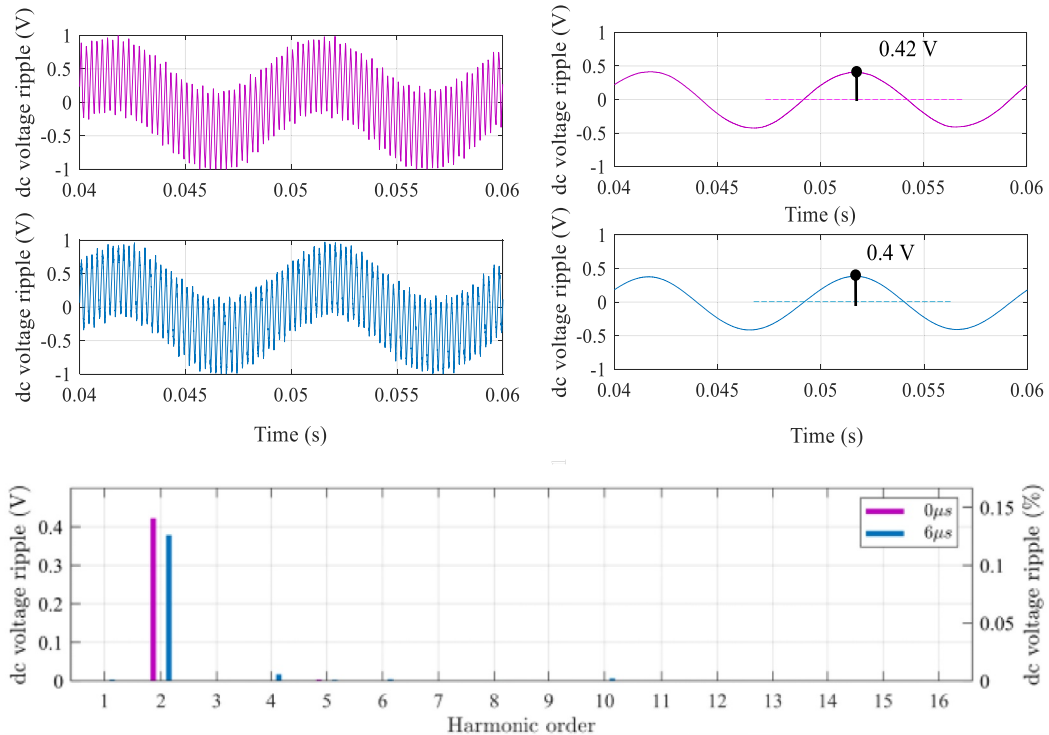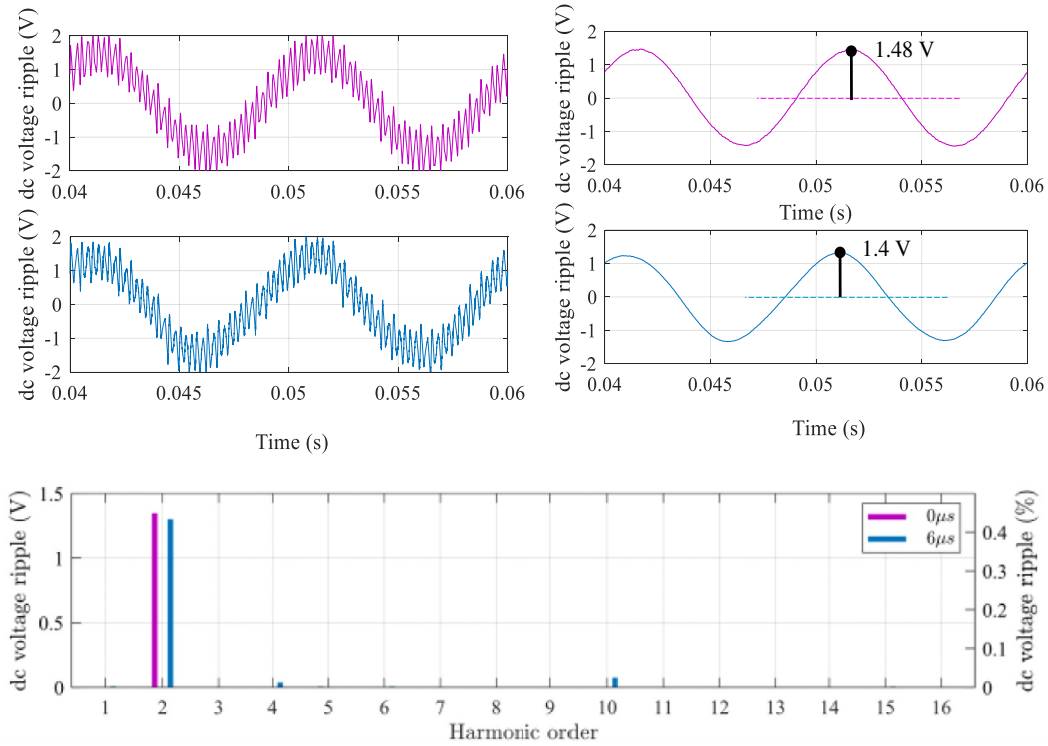

FIGURE 11 The total dc-link voltage ripple (top left) and its low-frequency component (top right): Simulations (pink traces) and experimental results (blue traces) over a fundamental period for $\varphi = 20°$, $m = 0.25$ (five-phase load). Bottom histogram shows harmonic spectra in case of no dead-time (pink lines) and 6 μs dead-time (blue lines)
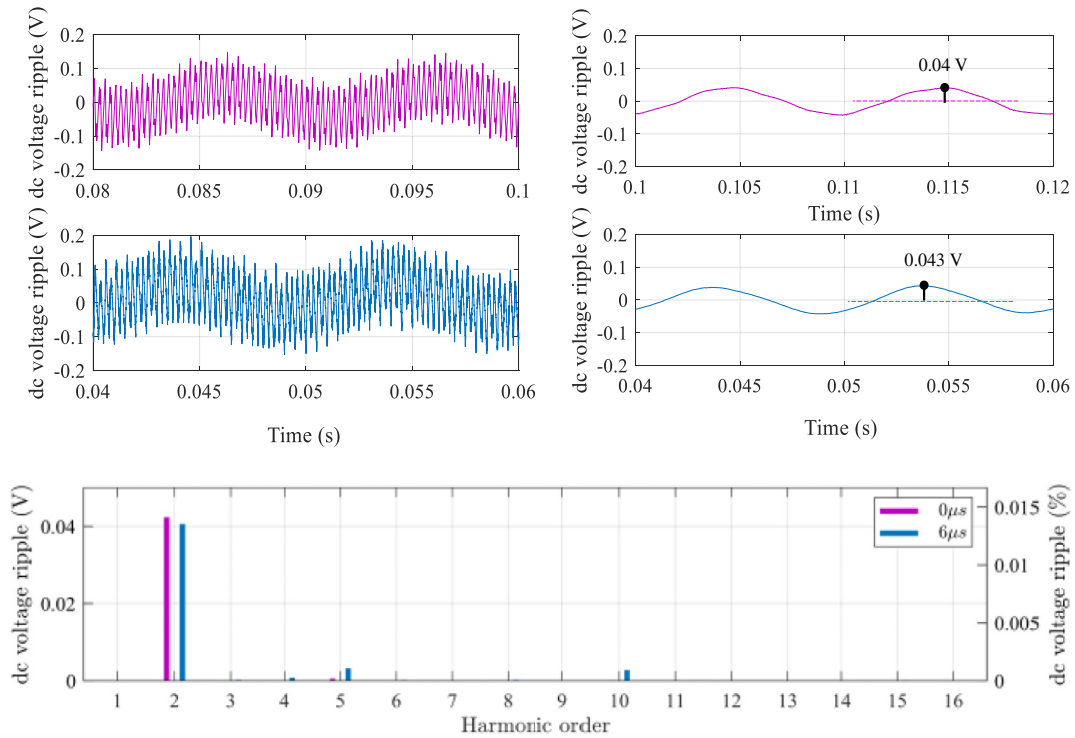
FIGURE 12 The total dc-link voltage ripple (top left) and its low-frequency component (top right): Simulations (pink traces) and experimental results (blue traces) over a fundamental period for $\varphi = 20°$, $m = 0.5$ (five-phase load). Bottom frame shows harmonic spectra in case of dead-time equal to 0 μs (pink histogram) and 6 μs (blue histogram)
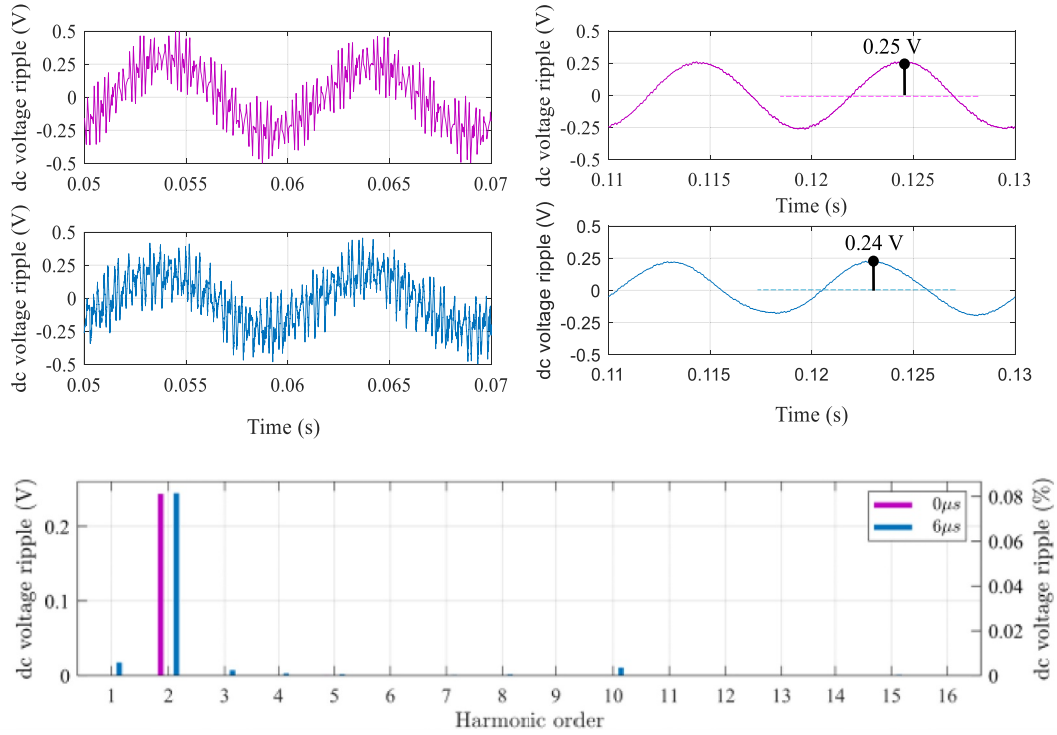

FIGURE 13 The total dc-link voltage ripple (top left) and its low-frequency component (top right): Simulations (pink traces) and experimental results (blue traces) over a fundamental period for $\varphi = 70°$, $m = 0.25$ (five-phase load). Bottom histogram shows harmonic spectra in case of no dead-time (pink lines) and 6 μs dead-time (blue lines)

FIGURE 14 The total dc-link voltage ripple (top left) and its low-frequency component (top right): Simulations (pink traces) and experimental results (blue traces) over a fundamental period for $\varphi = 70°$, $m = 0.5$ (five-phase load). Bottom histogram shows harmonic spectra in case of no dead-time (pink lines) and 6 μs dead-time (blue lines)

TABLE 6 Current sequence components of interest, unbalance factor and comparison within the dc voltage ripple amplitudes for different operating conditions (five-phase load)

φ	20°	20°	70°	70°
m	0.25	0.50	0.25	0.50
I_{+1} (A)	2.0427	3.7446	0.7866	1.5489
I_{-1} (A)	0.0742	0.1291	0.0071	0.0125
U_F (%)	3.6	3.45	0.90	0.81
ana. $\tilde{V}_{pk}$ (V)	0.42	1.48	0.04	0.25
sim. $\tilde{V}_{pk}$ (V)	0.42	1.48	0.04	0.25
exp. $\tilde{V}_{pk}$ (V)	0.40	1.40	0.04	0.24

three- and five-phase inverters. In fact, apart from small numerical noises, only a 14th order component is noticeable. Again, the small reduction in the second order harmonic component can also be justified by the small reduction in the output voltage/current introduced by the dead-time, according to Refs [30, 31].

6 | CONCLUSION

The dc-link voltage and current low-frequency ripple generated by a small degree of load unbalance in multiphase inverters

have been discussed in this work. In fact, even considering nominally balanced motors/loads, an undesired unbalance in order of a few percent is practically always present, introducing an instantaneous power oscillation at the double-fundamental frequency. This reflects in current and voltage low-frequency ripple on the dc-link inverter side, specifically, as a second-order harmonic component. The amplitudes of second-order harmonic components are calculated, and a simple guideline for designing the dc-link capacitor is proposed based on their amplitudes.

It has been found that, from the point of view of the dc-link capacitor sizing, if the same apparent power is considered within compared multiphase inverter topologies, there are no benefits of increasing the number of phases because the amplitude of the low-frequency voltage ripple component depends only on the level of unbalance (i.e. the unbalance factor).

Numerical simulations and experimental tests have been performed for three-, five- and seven-phase inverters considering different operating conditions. Presented results confirm the correctness of analytical developments and calculations for all the cases.

Further developments can consider investigating the unbalances of standard multiphase motors in their different operating conditions, that is, no-load, rated and/or partial load, transient conditions. In addition, a more detailed analysis of the dead-time effect on the dc-link voltage ripple can
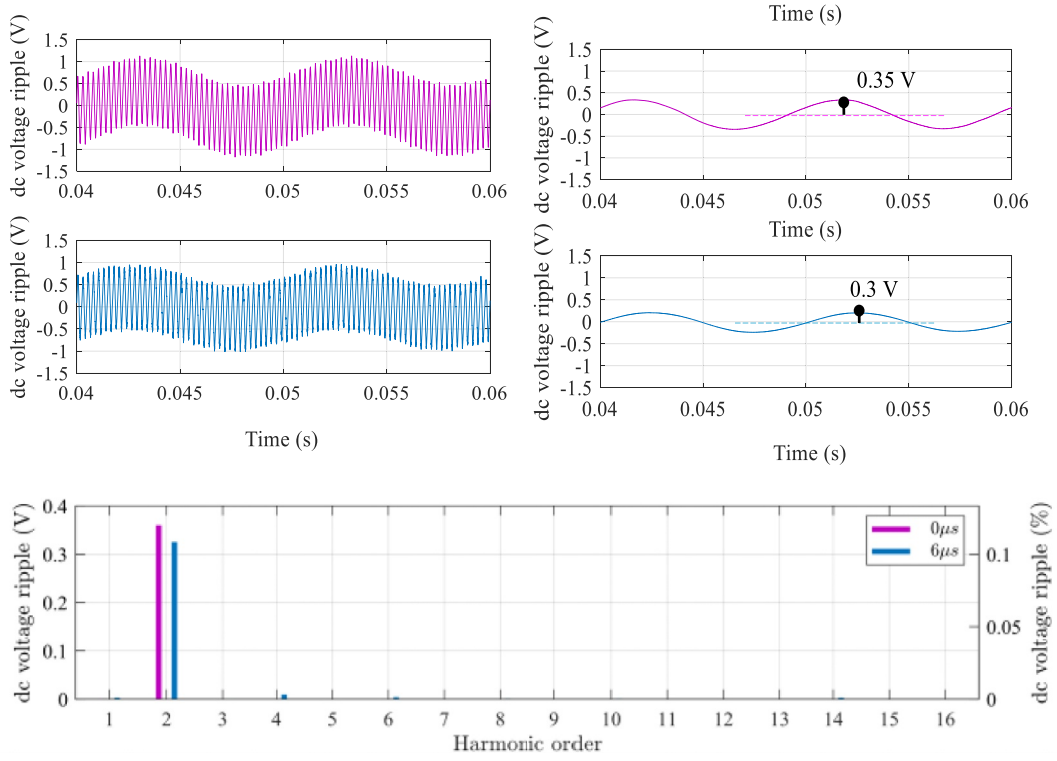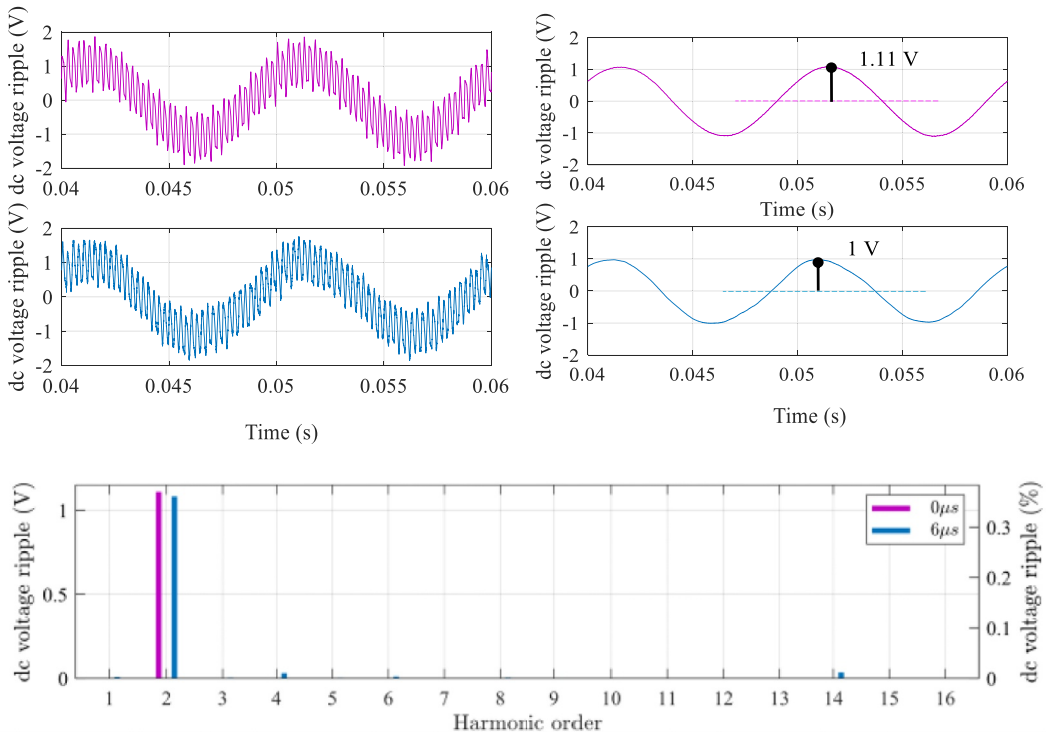
FIGURE 15 The total dc-link voltage ripple (top left) and its low-frequency component (top right): Simulations (pink traces) and experimental results (blue traces) over a fundamental period for $\varphi = 20°$, $m = 0.25$ (seven-phase load). Bottom frame shows harmonic spectra in case of dead-time equal to 0 μs (pink histogram) and 6 μs (blue histogram)

FIGURE 16 The total dc-link voltage ripple (top left) and its low-frequency component (top right): Simulations (pink traces) and experimental results (blue traces) over a fundamental period for $\varphi = 20°$, $m = 0.5$ (seven-phase load). Bottom histogram shows harmonic spectra in case of no dead-time (pink lines) and 6 μs dead-time (blue lines)
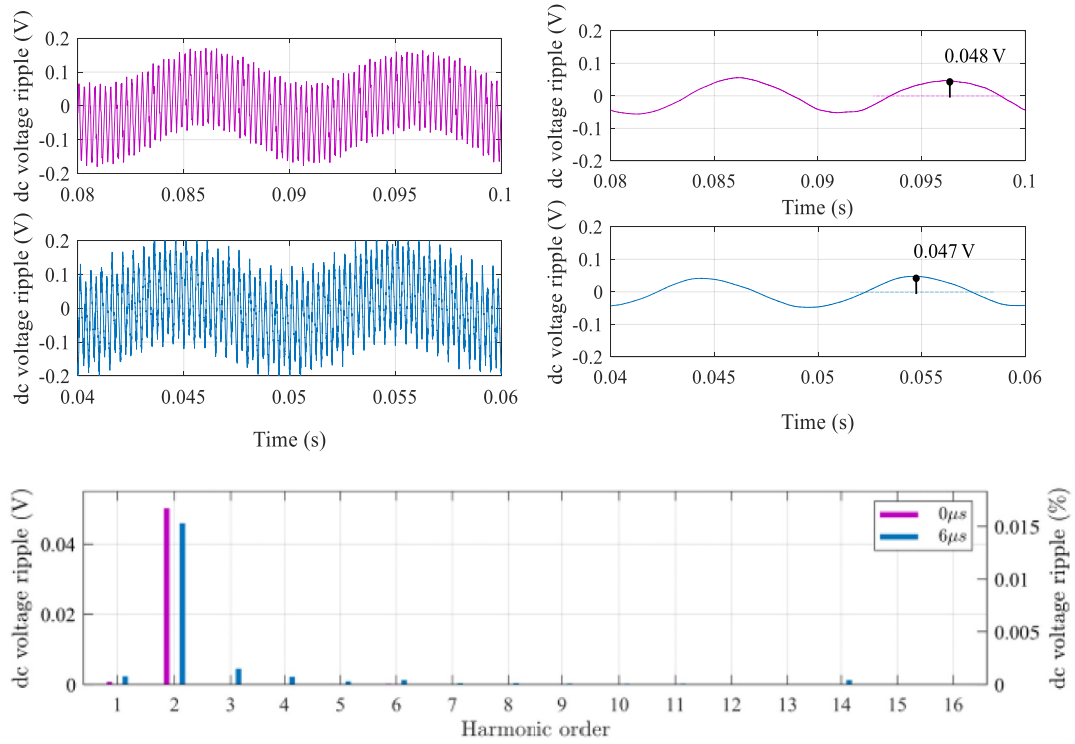
FIGURE 17 The total dc-link voltage ripple (top left) and its low-frequency component (top right): Simulations (pink traces) and experimental results (blue traces) over a fundamental period for $\varphi = 70°$, $m = 0.25$ (seven-phase load). Bottom histogram shows harmonic spectra in case of no dead-time (pink lines) and 6 μs dead-time (blue lines)
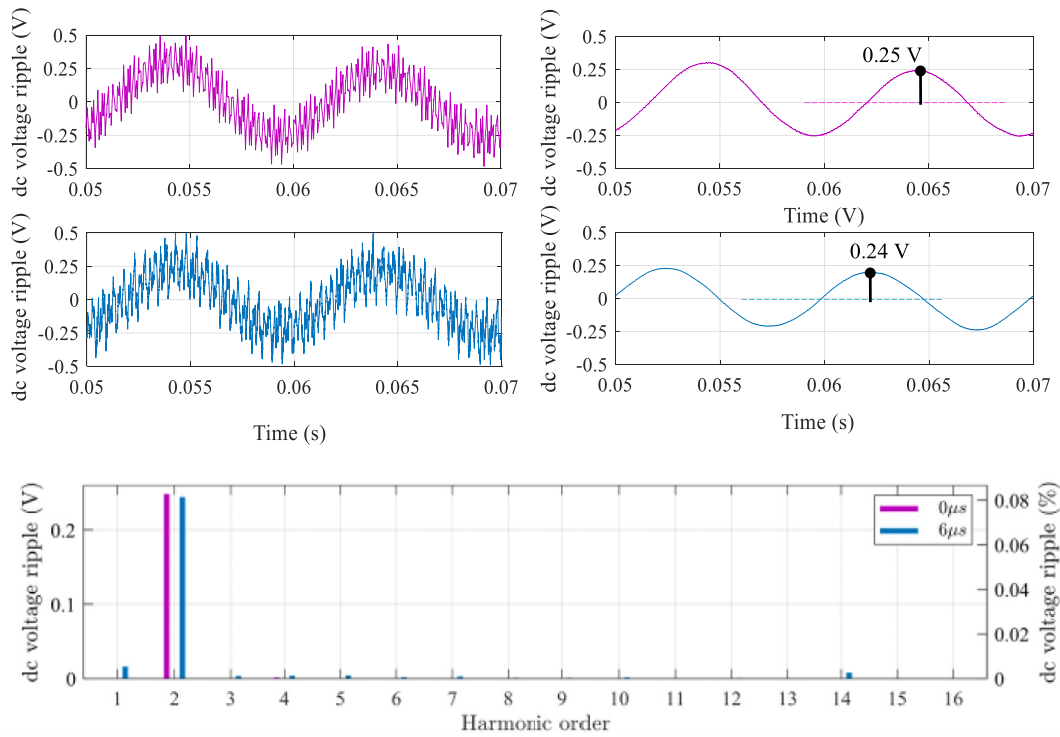

FIGURE 18 The total dc-link voltage ripple (top left) and its low-frequency component (top right): Simulations (pink traces) and experimental results (blue traces) over a fundamental period for $\varphi = 70°$, $m = 0.5$ (seven-phase load). Bottom histogram shows harmonic spectra in case of no dead-time (pink lines) and 6 μs dead-time (blue lines)

T A B L E 7 Current sequence components of interest, unbalance factor and comparison within the dc voltage ripple amplitudes for different operating conditions (seven-phase load)

φ	20°	20°	70°	70°
m	0.25	0.50	0.25	0.50
I_{+1} (A)	2.0474	3.6306	0.7842	1.5405
I_{-1} (A)	0.0420	0.0693	0.0083	0.0157
U_F (%)	2.05	1.91	1.06	1.02
ana. $\tilde{V}_{pk}$ (V)	0.33	1.11	0.050	0.25
sim. $\tilde{V}_{pk}$ (V)	0.35	1.10	0.048	0.25
exp. $\tilde{V}_{pk}$ (V)	0.30	1.00	0.047	0.24

be pointed out theoretically and experimentally, but based on the analysis of perfectly balanced load to avoid harmonic interferences.

ACKNOWLEDGEMENTS

CONFLICT OF INTEREST

There is not any conflict of interest.

DATA AVAILABILITY STATEMENT

Author elects to not share data.

ORCID

Marija Vujacic https://orcid.org/0000-0002-0446-4123
Obrad Dordevic https://orcid.org/0000-0002-6883-5237
Riccardo Mandrioli https://orcid.org/0000-0003-3015-4150
Gabriele Grandi https://orcid.org/0000-0002-4565-1064

REFERENCES

1. Levi, E.: Multiphase electric machines for variable speed applications. IEEE Trans. Ind. Electron. 55, 1893–1909 (2008)
2. Parsa, L.: On advantages of multi-phase machines. In: Proceedings of the IEEE IECON, Raleigh, NC, pp. 1574–1579. (2005)
3. Levi, E.: Advances in converter control and innovative exploitation of additional degrees of freedom for multiphase machines. IEEE Trans. Ind. Electron. 63, 433–448 (2016)
4. Casadei, D., et al.: A new carrier-based PWM strategy with minimum output current ripple for five-phase inverters. In: Proceedings of the 14th European Conference on Power Electronics and Applications (EPE), pp. 1–10. (2011)
5. Dujic, D., Jones, M., Levi, E.: Analysis of output current ripple rms in muliphase drives using space vector approach. IEEE Trans. Power Electron. 24(8), 1926–1938 (2009)
6. Jones, M., et al.: Switching ripple characteristics of space vector PWM schemes for five-phase two-level voltage source inverters- Part2: current ripple. IEEE Trans. Ind. Electron. 58(7), 2799–2808 (2011)
7. Grandi, G., Loncarski, J., Rossi, C.: Comparison of peak-to-peak current ripple amplitude in multiphase PWM voltage source inverters. In: Proceedings of the 15th IEEE Conference on Power Electronics and Applications, pp. 1–10. (2013)
8. Klima, J.: Analytical investigation of influence of DC-link voltage ripple on PWM fed induction motor drive. In: Proceedings of the IEEE Conference on Industrial Electronics and Applications, pp. 1–7. (2006)
9. Bierhoff, M.H., Fuchs, F.W.: DC-link harmonics of three-phase voltage-source converters influenced by the pulsewidth-modulation strategy-an analysis. IEEE Trans. Ind. Electron. 55, 2085–2092 (2008)
10. Deng, H., et al.: A general solution for theoretical harmonic components of carrier based PWM schemes. In: Proceedings of the IEEE Applied Power Electronics Conference and Exposition, pp. 1698–1703. (2009)
11. Kolar, J.W., Round, S.D.: Analytical calculation of the RMS current stress on the DC-link capacitor of voltage-PMW converter system. IEE Electr. Power Appl. 153(4), 535–543 (2006)
12. Dahono, P.A., Sato, Y., Kataoka, T.: Analysis and minimization of ripple components of input current and voltage of PWM inverters. IEEE Trans. Ind. Appl. 32, 945–950 (1996)
13. Vujacic, M., et al.: Analysis of dc-link voltage switching ripple in three-phase PWM inverters. Energies. 11, 471 (2018)
14. Pei, X., Zhou, W., Kang, Y.: Analysis and calculation of DC-link current and voltage ripples for three-phase inverter with unbalanced load. IEEE Trans. Power Electron. 30, 5401–5412 (2015)
15. Kueck, J.D., Casada, D.A., Otaduy, P.J.: A comparison of two energy efficient motors. IEEE Trans. Energy Convers. 13(2), 140–146 (1998)
16. Albadi, M.H., et al.: Unbalance in power systems: Case study. In: Proceedings of the IEEE International Conference on Industrial Technology, ICIT, (2015)
17. Wang, H., et al.: The impact of grid unbalances on the reliability of dc-link capacitors in a motor drive. In: Proceedings of the IEEE Energy Conversion Congress and Exposition, pp. 4345–4350. (2017)
18. Lee, K., et al.: DC-bus electrolytic capacitor stress in adjustable-speed drives under input voltage unbalance and sag conditions. IEEE Trans. Ind. Appl. 43(2), 495–504 (2007)
19. Vujacic, M., Dordevic, O., Grandi, G.: Evaluation of dc-link voltage switching ripple analysis in multiphase PWM voltage source inverters. IEEE Trans. Power Electron. 35(4), 3478–3490 (2020)
20. Bojoi, R., et al.: Computation and measurements of the DC link current in six-phase voltage source PWM inverters for AC motor drives. In: Proceedings of the Power Conversion Conference, pp. 953–958. (2002)
21. Rouhaba, N., Semail, E., Duguey, J.F.: Impact of PWM strategies on RMS current of the dc-link voltage capacitor of a dual-three phase drive. In Proceedings of the IEEE Vehicle Power and Propulsion Conference, pp. 1–7. (2014)
22. Dahono, P.A., et al.: Input ripple analysis of five-phase pulse width modulated inverters. IET Power Electron. 3, 716–723 (2010)
23. Vujacic, M., et al.: Evaluation of DC-link voltage ripple in five-phase PWM voltage source inverters. IET J. Eng. 2019(17), 3709–3714 (2019)
24. Vujacic, M., Dordevic, O., Grandi, G.: Evaluation of DC-link voltage ripple in seven-phase PWM voltage source inverters. In: Proceedings of the IEEE International Telecommunications Energy Conference (2018)
25. Muqorobin, A., Dahono, P.A., Purwadi, A.: Optimum phase number for multiphase PWM inverters. In: Proceedings of the IEEE Conference on Electrical Engineering, Computer Science and Informatics, pp. 1–6. (2017)
26. Grandi, G., Serra, G., Tani, A.: General analysis of multi-phase systems based on space vector approach. In: Proceedings of the International Power Electronics and Motion Control Conference, pp. 834–840. (2006)
27. Pilley, P., Manyage, M.: Defintions of voltage unbalance. IEEE Power Eng. Rev. Mag. 5, 50–51 (2001)

28. Pillay, P., Hofman, P., Manyage, M.: Derating of induction motors operating with a combination of unbalanced voltages and over- or undervoltages. IEEE Trans. Energy Convers. 17(4), 485–491 (2002)

29. Guha, A., Narayanan, G.: Impact of dead time on inverter input current, DC-link dynamics, and light-load instability in rectifier-inverter-fed induction motor drives. IEEE Trans. Ind. Appl. 54(2), 1414–1424 (2018)

30. Grandi, G., Loncarski, J.: Space vector analysis of dead-time voltage distortion in multiphase inverters. In: Proceedings of the IEEE International Power Electronics and Motion Control Conference, EPE-PEMC 2012 ECCE Europe, pp. DS3c.6-1–DS3c.6-7. (2012)

31. Jones, M., et al.: Dead-time effects in voltage source inverter fed multiphase AC motor drives and their compensation. In: Proceedings of 13th European Conference on Power Electronics and Applications, EPE, pp. 1–10. (2009)